Journal of Electrical and Computer Engineering Innovations
(JECEI)
Journal homepage: http://www.jecei.sru.ac.ir

Research paper

A Public Information Precoding for MIMO Visible Light Communication System Based on Manifold Optimization

H. Alizadeh Ghazijahani [*]***, M. Atashbar***

Department of electrical engineering, Azarbaijan Shahid Madani University, Tabriz, Iran.

Article Info

Article History:
Received 04 September 2024
Reviewed 06 November 2024
Revised 10 December 2024
Accepted 16 December 2024

Keywords:
VLC
MIMO
Precoding
Public information
Optimization

[*]Corresponding Author's Email Address:
hag@azaruniv.ac.ir

Abstract

Background and Objectives: The combination of multiple-input-multiple-output (MIMO) with a Visible light communication (VLC) system leads to a higher speed of data transmission named the MIMO-VLC system. In multi-user (MU) MIMO-VLC, an LED array transmits signals to users. These signals are categorized as signals of private information for each user and signals of public information for all users.
Methods: In this research, we design an omnidirectional precoding to transmit the signals of public information in the MU-MIMO-VLC network. We aim to maximize the achievable rate which leads to maximizing the received mean power at the possible location of the users. Besides maximizing the achievable rate, we consider equal mean transmission power constraints in all LEDs to achieve higher power efficiency of the power amplifiers used in the LED array. Based on this, we formulate an optimization problem in which the constraint is in the form of a manifold, and utilize a gradient method projected on the manifold to solve the problem.
Results: Simulation results indicate that the proposed omnidirectional precoding can achieve superior received mean power besides more than 10x bit error rate reduction compared to the classical form without precoding utilization.
Conclusion: In this research, we proposed an omnidirectional precoding for transmitting the public signals in the MU-MIMO-VLC system. The proposed optimization problem maximizes the received mean power constrained with equal transmission mean power of LEDs in the array.

Introduction

Visible light communication is one of the attractive optical communication systems that utilize the visible region of optical spectrum [1]. Due to the combination of communication with lighting, VLC is one of the emerging technologies in 6G and regarded as a promising technique to provide internet in indoor wireless access [2]. Generally speaking, VLC has many significant advantages, such as license-free spectrum, high security, high data rates, low cost, and freedom from hazardous electromagnetic radiation [3], [4].

Furthermore, multiple-input-multiple-output (MIMO) techniques are used in communication systems to ensure a high data rate and reliability where transmitters and receivers use multiple antennas [5]. A special case of MIMO systems is multi-user MIMO (MU-MIMO) where the transmitter/receiver is equipped with multiple antennas and the receiver/transmitter consists of multiple users with single or multiple antennas. In this case, a base station (BS) with an antenna array supports multiple mobile stations (MS) simultaneously [6].

Recently, to jointly benefit from the advantages of VLC and MU-MIMO, MU-MIMO-VLC systems have been considered, in which a LED array is used to transmit the downlink signals to multiple users simultaneously [7], [8]. To prevent inter-user interference, the users' associated signals are precoded before transmission [9]-[18]. This type of precoding is named directional precoding where the precode matrix is designed based on the channel matrix. The authors in [9] have formulated the precoding and power allocation problems and do energy efficiency optimizations for multi-cell rate-splitting multiple access VLC systems.

In [10], C. Wang *et al.* proposed a precoding based on successive interference cancellation (SIC) to optimize the electrical/optical power of each LED and achieve the maximum sum rate. Another research designed a precoding matrix by maximizing mutual information subject to both peak and average power constraints [12]. The performance of MU-MIMO-VLC block diagonalization precoding is discussed in [13]. The results show that inter-user interference is eliminated and the complexity of users' terminals is reduced. Another research on precoding for MU-VLC is reported in [14] in which the confidentiality of users' messages has been considered.

In a MU communication system, each user has its private information. The above-mentioned and similar literature [10]-[14] employ precoding techniques to send private information to mitigate the other user's signal by maximizing the received signal strength at the intended user. Applying precoding needs to know the channel state information (CSI) of each user. Furthermore, the transmitter unit broadcasts specific public or common information concurrently to all users connected to the network. This information includes data for synchronization, medium access control frames, link recovery request, or when an IP address is dynamically assigned to a device [19]. To transmit such information, it is assumed that the user location is not known, so the user location feedback is not needed.

While the rate-splitting multiple access (RSMA) technique enables the concurrent transmission of specific common information and private data in a VLC network [20], [21].

However, in the context of RSMA, the term "common information" is defined as a message that, while meant for a particular user, must be decoded by all users. This understanding contrasts sharply with the concept of a public message, which necessitates that all users have access to the information it conveys [22]. In addition, similar to directional precoding, in RSMA, CSI is needed in the precoding of both common and private information to prevent inter-user interference.

On the other hand, the public message needs to be broadcast to all possible user locations, so inter-user interference is not a challenge here. In this case, we need an efficient precoding for the transmission signal to balance the received signal over the whole coverage area. This type of precoding is named omnidirectional precoding [23], [24]. The main differences between omnidirectional and directional precoding can be summarized as: 1) The transmit information in directional precoding is private information of that user while in omnidirectional precoding, the transmit information is the public information that all users wish to receive, 2) Directional precoding relies on the precise knowledge of the channel vector that exists between the user and the transmitter array. In contrast, omnidirectional approaches require only the channel model without the need for specific vector values, 3) in the directional precoding, the transmitted energy of LEDs is concentrated in the target point where the user is located there. In comparison, the idea in omnidirectional precoding (assuming an unknown user location) is to maximize the received energy in all potential user locations. To the best of our knowledge, there is not any study that addresses the design of omnidirectional precoding proportional to MU-MIMO-VLC systems.

In this paper, we present an omnidirectional precoding algorithm for a transmitter LED array in a MU indoor MIMO-VLC system for the transmission of public information in the network.

A comparison of the fundamental differences between introduced omnidirectional precoding for VLC and traditional directional precoding are outlined in Table 1.

To this end, while the user location is not known, we propose to maximize the achievable rate in user potential locations which leads to maximizing the received mean power at the whole area. On the other hand, to achieve higher power efficiency of the power amplifiers used in the LED array, it is needed that the mean transmission powers of the signals associated with all LEDs be the same. Consequently, we consider this constraint besides maximizing the achievable rate in our problem. This leads to a constrained optimization problem in which the constraint is in the form of manifold. Accordingly, to solve this problem, we propose a gradient method projected on the manifold.

The rest of this paper is organized as follows. The system model is described in the next section. After

that we propose our optimization problem. The simulation setup, results, and discussion are presented and finally, the paper is concluded.

Table 1: Fundamental differences between directional and proposed omnidirectional precoding for VLC

Symbol	Directional Precoding	Omnidirectional Precoding
Scope	Transmitting specific signal to each user	Transmitting signal to all users simultaneously
Data	private	public
Design requirements	CSI values for each transmitter-user pair	Channel model
Scattered Power distribution	Concentrated to the user location	Distributed over possible locations of users
Objective function	Maximizing the signal to interference plus noise ratio	Maximizing the received mean power of possible locations of users

System Model

Consider a VLC-MIMO system with a uniform rectangular LED array to broadcast public information to the single photo-diode (PD) equipped users in the coverage area shown in Fig. 1 assuming that the array of LEDs consists of M_t LEDs in a rectangular structure as $M_t = M_x \times M_y$ on the x-y plane and d_x and d_y are the distances of adjacent LEDs along the *x*-axis and *y*-axis, respectively. Note that in our model, the LED panel is placed on the ceiling with height *D* from the room's floor. Furthermore, assume that the public information signal vector $\boldsymbol{s} = [s_1, s_2, \dots s_q]^T$ sent to users, where s_i, q, and $(.)^T$ indicate the *i*-th transmitted symbol, number of symbols, and transpose, respectively. This signal vector is multiplied by the designed precoding matrix $\boldsymbol{P} = [\boldsymbol{p}_1, \boldsymbol{p}_2, \dots \boldsymbol{p}_{M_t}]^T \in \mathbb{R}^{M_t \times q}$ to generate LEDs' transmission signal vector $\boldsymbol{v} = \boldsymbol{P}\boldsymbol{s} + e$, where $\boldsymbol{v} = [v_1, v_2, \dots v_{M_t}]^T$ with v_i presents the transmit signal of *i*-th LED located in (x_i, y_i, D)

$$x_i = \left\lfloor \frac{i-1}{M_y} \right\rfloor d_x \,, y_i = (i \bmod M_y - 1) d_y \,, \quad i = 1, 2, \dots M_t \,, \tag{1}$$

in which $\lfloor . \rfloor$ denotes the floor operator sign and 'mod' indicates the reminder of deviation and *e* is the DC offset to confirm non-negative elements of $\boldsymbol{v}$.

In VLC systems, each user is equipped with a PD to receive the transmitted optical signal strength from LEDs array. Thus, the received signal at the *j*-th user in the coordinates (x_j^u, y_j^u, h) will be as follows [12]:

$$r_j = \boldsymbol{h}_j^T (\boldsymbol{P}\boldsymbol{s} + e) + n \,, \tag{2}$$

where $\boldsymbol{P}$ is the $M_t \times q$ precoding matrix, *n* is white Gaussian noise and $\boldsymbol{h}_j$ is the $M_t \times 1$ channel vector. $\boldsymbol{h}_j = [h_{j1}, h_{j2}, \dots h_{jM_t}]^T$ with h_{ji} is the VLC channel gain between the *i*-th LED and the *j*-th user.

VLC channel models are currently investigated under two categories: deterministic and stochastic models. Deterministic models aim to predict channel characteristics at a specific location of the transmitter and receiver, as well as the surrounding environment, with ray tracing, recursive, and empirical algorithms. In stochastic approaches, the impulse responses of VLC channels are defined by the law of light propagation applied to a specific geometry of transmitter, receiver, and scattered [25]. In this research, we also use deterministic channel model as commonly used in other literature.

As the line of sight (LOS) channel of the optical wireless channel contains most parts of the transmitted energy [10], we ignore the non-LOS part in this work. We use the well-known Lambertian model to estimate the path loss in VLC channel. Consequently, according to the geometry presented in Fig. 1, for the LOS path, h_{ji} is given as [26]

$$h_{ji} = \begin{cases} \frac{A_d (m_l+1)}{2\pi d_{ji}^2} \cos^{m_l}(\phi_{ji}) \cos(\theta_{ji}) TG & if \;\; 0 \le \theta_{ji} \le \psi_R \\ 0 & if \;\; \theta_{ji} < \psi_R \end{cases}, \tag{3}$$

where ϕ_{ji} denotes the emitting angle, θ_{ji} denotes the incident angle from the *i*-th LED to *j*-th user, A_d denotes the area of the receiver PD, m_l is Lambert's mode number expressing the directivity of the source beam, the T denotes the signal transmission coefficient of an optical filter, ψ_R denotes the field of view of the receiver PD, G denotes the concentrator gain, and d_{ji} is the distance between *i*-th LED to *j*-th user PD [26]. Given the significant attenuation observed in this model relative to distance, the impact of multipath reflections on the received signal is negligible and can therefore be disregarded.

Proposed Optimization

In this paper, the idea is to design an omnidirectional precoding matrix for efficient transmission of public information signals of all users distributed on the coverage area in the VLC network. To address this challenge appropriately, two limitations are considered. 1) Maximum achievable rate, 2) constant mean transmission power of array LEDs.

A. Maximum Achievable Rate

According to the channel model described in (2), the mutual information of MIMO-VLC downlink transmission after DC suppression will be as follows [27], [28]

$$I_j = \log\left(1 + \frac{1}{\delta^2}\boldsymbol{h}_j^H \mathbf{P}\mathbf{P}^H \boldsymbol{h}_j\right), \quad (4)$$

in which δ^2 indicate the variance of noise at the receiver and $(.)^H$ indicates the Hermitian. Besides, it is supposed that the mean power of the elements of the vector $\boldsymbol{s}$ is equal to one. According to (4), maximizing term $\boldsymbol{h}_j^H \mathbf{P}\mathbf{P}^H \boldsymbol{h}_j$ leads to maximum achievable rate where it is in line with maximizing received mean power at the *j*-th user. Since the users can be located at any point of the covered area, so the precoding matrix should be designed in a way that term $\boldsymbol{h}_j^H \mathbf{P}\mathbf{P}^H \boldsymbol{h}_j$ achieves its maximum value for all possible h_j values.

To this aim, first, we do sampling from the coverage area uniformly, so that the work plane seems as a grid surface with step d_g. Given this premise, $\boldsymbol{h}_j$ is defined as the channel vector between the LED array and the *j*-th point on the grid surface, and N_s denotes the total number of grid points. Then we maximize the average of received mean power (ARMP) at the sampled location points as

$$ARMP = \frac{1}{N_s M_t}\sum_{j=1}^{N_s} \boldsymbol{h}_j^H \mathbf{P}\mathbf{P}^H \boldsymbol{h}_j . \quad (5)$$

In this equation, the parameter M_t is utilized to normalize the total transmit power at the LED array.

B. Keeping Constant the Mean Transmission Power of Leds in the Array

In a similar way to the radio frequency MIMO transmission system [28], to achieve a higher power efficiency of the amplifiers used to drive the LED array, it is needed that the mean transmission powers of the signals associated with all LEDs be the same. Supposing the elements of $\boldsymbol{s}$ are independent with zero-mean and unit variance, the mean transmission power of the *i*-th LED can be stated as

$$E(\boldsymbol{v_i^2}) = E\left(\left(\boldsymbol{p_i^T s} + e\right)^2\right)$$
$$= \boldsymbol{p_i^T E(ss^T) p}_i + e^2 = \boldsymbol{p_i^T\, p}_i + e^2 , \quad (6)$$

in which $E(.)$ stands for expectation operator. In (6), the first term is the mean of AC power and the second one is DC power. To keep constant the mean transmit power of all LEDs, $\boldsymbol{p_i^T\, p}_i$ must be constant for $i = 1, 2, \ldots M_t$. Without loss of generality, we get $\boldsymbol{p_i^T\, p}_i = 1$ as a constraint of problem where can be expressed in the matrix form as follows

$$diag(\boldsymbol{P}\boldsymbol{P}^{\boldsymbol{H}}) = \boldsymbol{I}_{M_t} , \quad (7)$$

in which, $\boldsymbol{I}_{M_t}$ is the $M_t \times M_t$ identity matrix and $diag(.)$ represents a diagonal matrix whose major diagonal elements are equal to the major diagonal elements of the matrix. Accordingly, the proposed constrained optimization problem to design the precoding matrix $\boldsymbol{P}$ is

$$\max_{\boldsymbol{P}} \quad \sum_{j=1}^{N_s} \boldsymbol{h}_j^H \mathbf{P}\mathbf{P}^H \boldsymbol{h}_j$$
$$s.t. \quad diag(\boldsymbol{P}\boldsymbol{P}^{\boldsymbol{H}}) = \boldsymbol{I}_{M_t} . \quad (8)$$

As the term $\sum_{j=1}^{N_s} \boldsymbol{h}_j^H \mathbf{P}\mathbf{P}^H \boldsymbol{h}_j$ is a concave function, by choosing $(\boldsymbol{P}) \triangleq -\sum_{j=1}^{N_s} \boldsymbol{h}_j^H \mathbf{P}\mathbf{P}^H \boldsymbol{h}_j$, it transforms to a convex function. Accordingly, the optimization problem forms as

$$\min_{\boldsymbol{P}} \quad f(\boldsymbol{P})$$
$$s.t. \quad diag(\boldsymbol{P}\boldsymbol{P}^{\boldsymbol{H}}) = \boldsymbol{I}_{M_t} . \quad (9)$$

Recently, geometric solutions are used to solve various optimization problems. One kind of such solutions is manifold-based geometry which is used in constrained optimization problems [30], [31] because of its relative simplicity and optimality. The constraints in constrained optimization problems can be interpreted as isolated points in the space that are in the manifold forms such as Stiefel, Grassmann, Riemannian, etc. Consequently, the optimum points are searched in the space that is inside the manifold.

In this work, we propose a manifold-based method to solve (9). As the constraint in (9) is in the form of Grassmann manifold [30] and $f(\boldsymbol{P})$ is in the form of a quadratic function (a convex function), we use the gradient method projected on the manifold, in which, matrix $\boldsymbol{P}$ is calculated iteratively as

$$\boldsymbol{P}_{k+1} = \boldsymbol{P}_k - \mu \nabla f(\boldsymbol{P}_k) , \quad (10)$$

in which $\boldsymbol{P}_k$ is the $\boldsymbol{P}$ values in *k*-th iteration, μ is step size, and $\nabla f(\boldsymbol{P})$ is the $M_t \times q$ gradient matrix of $f(\boldsymbol{P})$. According to matrix relations on [32], we have

$$\nabla f(\boldsymbol{P}) = -2\sum_{j=1}^{N_s} \boldsymbol{h}_j \boldsymbol{h}_j^H \boldsymbol{P} . \quad (11)$$

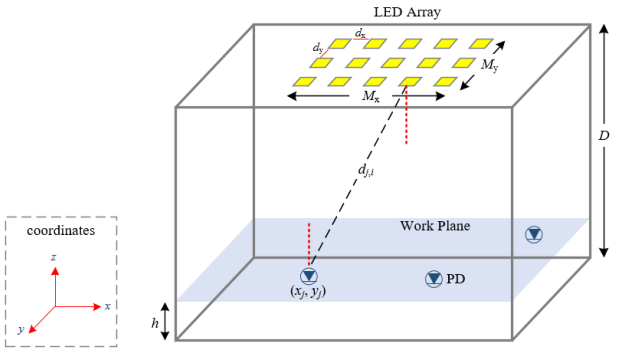

Fig. 1: Proposed system model.

In each iteration of the gradient algorithm, to ensure the constraint is established, the resulting matrix $\boldsymbol{P_{k+1}}$ is projected on the manifold. Since the constraint in (9) is in the form of the Grassmann manifold, the projection on the above manifold is as [30]

$$\boldsymbol{P}_{k+1} \leftarrow \left(diag(\boldsymbol{P}_{k+1}\boldsymbol{P}_{k+1}^{H})\right)^{-\frac{1}{2}} \boldsymbol{P}_{k+1} . \quad (12)$$

The iteration is continued until the difference of $f(\boldsymbol{P}_k)$ goes below a determined small value ε for two successive iterations to satisfy the convergence condition, as $|f(\boldsymbol{P}_{k+1}) - f(\boldsymbol{P}_k)| < \varepsilon$. The steps of the proposed algorithm to solve the optimization problem (9) are determined by the projected gradient method on the manifolds presented in Algorithm 1.

Algorithm 1: Solving the optimization problem presented in (9)

1- Initialization of matrix $\boldsymbol{P}$
2- Calculate $\nabla f(\boldsymbol{P})$ using (11)
3- Update $\boldsymbol{P}$ as (10)
4- Project $\boldsymbol{P}$ on the manifold based on (12)
5- Repeat steps 2-4 to achieve the convergence condition

Results and Discussion

In this section, we present the simulation setup and results to show how the proposed precoding algorithm for MIMO-VLC satisfies two limitations stated in section 2.

To this end, we consider optimized ARMP as an evaluation criterion in which optimized ARMP is defined as the value of ARMP based on the designed precoding matrix $\boldsymbol{P}$. To the best of our knowledge, there is not any similar study to design an omnidirectional precoding matrix for MIMO-VLC system, we choose the mean of ARMP parameters over all random precoding matrix $\boldsymbol{P}$ as a reference method to compare the results. We name this as 'classical method'. We utilize RSMA criterion to evaluate the performance of the proposed omnidirectional precoding. Since, RSMA is proportional to achievable rate parameter, we discuss the performance of the system with this criterion.

In the simulation, we consider a scenario in which a LED panel with uniform rectangular array is supposed to be installed in the center of the room ceiling.

Also, the users can be placed at all possible locations on the floor of the room and each of them receives the VLC signal emitted from all LEDs.

As mentioned in section 3, to aim for maximum achievable rate, we need to do sampling from all possible locations of users, therefore, in our simulations, the floor of the room is sampled uniformly with a distance of 0.1 in both axes. The other simulation parameters are summarized in Table 2.

Table 2: Simulation parameters

Symbol	Description	Value
-	room dimensions [width, length, height]	[5, 6, 3] m
$\boldsymbol{\psi_R}$	receiver field of view	75°
$\boldsymbol{A_d}$	receiver area	1×10^{-4} m^2
$\boldsymbol{m_l}$	Lambert's mode number	1
$\boldsymbol{T_s(\theta_T)}$	signal transmission coefficient of an optical filter	1
$\boldsymbol{g(\theta_T)}$	concentrator gain	5
$\boldsymbol{\varepsilon}$	stop parameter in iterative algorithm	10^{-4}
$\boldsymbol{q}$	number of symbols	10
$\boldsymbol{d_g}$	Work plane grid step	1 mm

A. Convergence of Optimization Problem

In the first simulation, the convergence of the gradient method projected on the manifold in solving the proposed optimization problem is investigated. In this way, a 3×3 LED rectangular array with a distance of 0.02 m between adjacent elements is considered at the ceiling and the PD of users is located on a flat surface, named work plane, with height 1m from the floor. The $f(\boldsymbol{P})$ value is calculated in each iteration. The result shown in Fig. 2 indicates that the cost function is converged in 5-th iteration. The resultant precoding matrix in 5-th iteration is as (13) showing that the constraint of proposed optimization problem

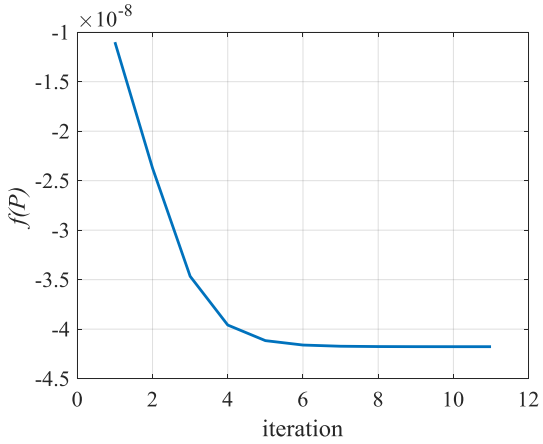

Fig. 2: Convergence of proposed algorithm over iterations.

$$\boldsymbol{P}=\begin{bmatrix} 0.485532 & 0.389968 & 0.148727 & -0.28536 & 0.032314 & 0.279723 & -0.33371 & 0.459929 & -0.06347 & 0.320037 \\ 0.063389 & -0.5254 & -0.0869 & 0.357057 & -0.25406 & -0.22072 & 0.185637 & 0.187258 & -0.33472 & -0.53857 \\ -0.29119 & -0.13221 & -0.16466 & -0.47472 & 0.395979 & 0.432586 & 0.102007 & 0.273667 & -0.21922 & -0.40984 \\ 0.031884 & -0.35761 & -0.07127 & -0.35639 & 0.424023 & -0.39309 & 0.287618 & -0.14704 & -0.4282 & 0.342038 \\ 0.243148 & -0.38668 & -0.15495 & -0.31892 & -0.39669 & -0.3259 & -0.21353 & -0.09049 & -0.49624 & 0.319427 \\ -0.37737 & -0.4311 & 0.093535 & -0.22487 & 0.246277 & 0.378553 & 0.145202 & 0.385867 & 0.450226 & -0.1892 \\ -0.45466 & -0.23233 & 0.337457 & 0.352245 & -0.43656 & 0.389548 & 0.377869 & 0.004552 & 0.058183 & 0.113256 \\ -0.46861 & 0.191308 & 0.274291 & -0.32424 & -0.51558 & -0.02095 & -0.12132 & -0.41916 & -0.05102 & 0.322735 \\ 0.087989 & 0.13417 & -0.16224 & -0.12184 & 0.365285 & 0.004531 & 0.209953 & 0.693242 & -0.44237 & 0.281573 \end{bmatrix}. \quad (13)$$

presented in (8) is satisfied. As the $f(\boldsymbol{P})$ is a well-known quadratic convex function, the convergence of Gradient descent algorithm is guaranteed. Consequently, the convergence curve of proposed algorithm presented in Fig. 2 is gained through simulation.

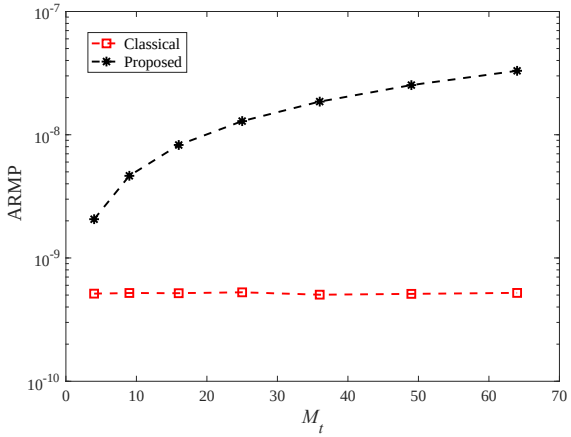

Fig. 3: The ARMP of classical and proposed methods versus number of LEDs in the array with d_x = 0.05 m.

B. Number of LED Array Elements

In the second simulation, the behavior of ARMP versus different LED numbers in the array is investigated. In this simulation the parameters are set as d_x = 0.01, h = 2.5 m, and M_t the number of LEDs varies from 4 to 64. Fig. 3 shows that the ARMP of the proposed method is improved by increasing the number of LEDs, while the classical ARMP is constant over M_t changes, as expected. This is due to the fact that as the elements of $\boldsymbol{P}$ matrix are chosen randomly and according to the law of large numbers, the ARMP is proportional to the variance of $\boldsymbol{P}$ elements. Based on the considered parameters in simulation, the ARMP value for the classical method is almost fixed at 5.2×10^{-10} for all M_t values.

This is while, for the proposed method the ARMP is 4.6×10^{-9} and 3.3×10^{-8} for M_t = 9 and 64, respectively. The received signals from LEDs at each user location sum up linearly in classical method which is not necessarily constructive while, the designed precoding leads to a constructive summation of LEDs' signals in the proposed method. By increase in M_t, the degree of freedom in the constructive summation is increased and helps to increase optimized ARMP.

C. Distance between LED Array Elements

To investigate the impact of distance between LEDs in the array, we repeated the simulation for $d_x = d_y \in \{0.01, 0.02, \ldots, 0.1\}$.

The ARMP versus different distance values is depicted in Fig. 4. In this figure, the simulation results for the proposed method are presented with three different numbers of LEDs in the array. Besides, the ARMP curve for the classical method for any arbitrary M_t is depicted versus d_x. As seen, the ARMP values remain unchanged by increasing in d_x in both methods. The constant value of ARMP is due to the low dynamic range of d_x.

The simulation is repeated for both varying d_x and d_y for proposed method under $M_t \in \{9, 25, 64\}$ and classical method. The results are shown in Fig. 5 where a near flat surface is appears for each structure with M_t LEDs.

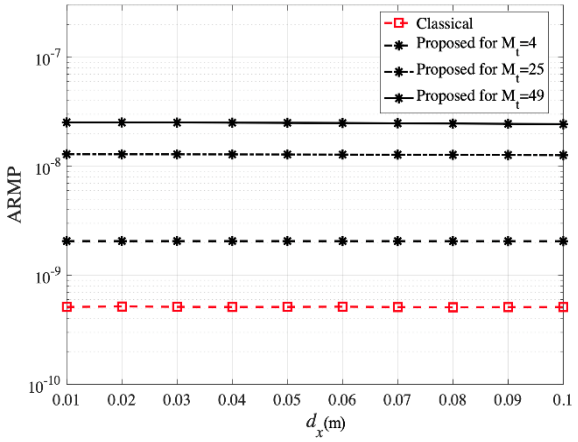

Fig. 4: The ARMP of proposed method under $M_t \in \{9, 25, 64\}$ and classical method versus low dynamic range adjacent distance between LEDs in the array.

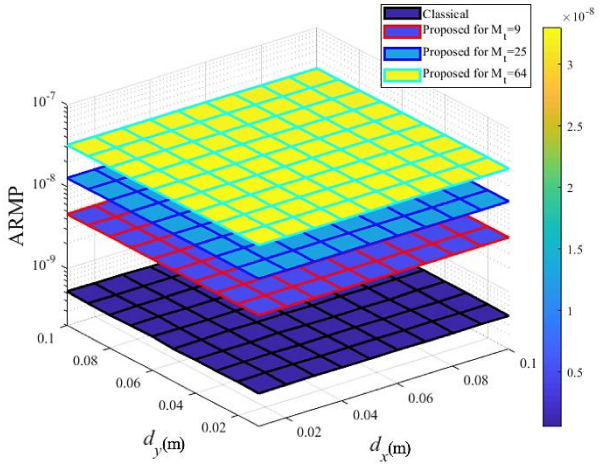

Fig. 5: The ARMP of proposed method under $M_t \in \{9, 25, 64\}$ and classical method versus low x and y axis dynamic range adjacent distances between LEDs in the array in.

To more investigation, the simulation is repeated for a d_x with a high dynamic range where the results are shown in Fig. 6. As seen, for large M_t, the ARMP curve of the proposed method falls by an increase in d_x while it is almost constant for small M_t's. This is due to the fact that when the M_t and d_x are concurrently large, the physical length of LED array (panel) goes expand over the ceiling and this makes the constructive combination of LED signals hard in most points of the work plane.

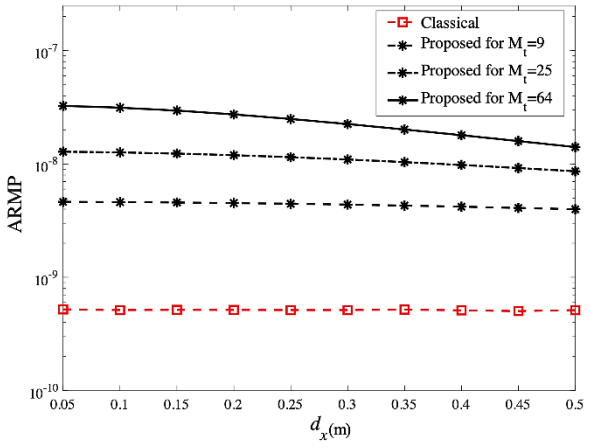

Fig. 6: The ARMP of proposed method $M_t \in \{9, 25, 64\}$ and classical method versus high dynamic range adjacent distance between LEDs in the array.

Similar to low dynamic range by varying d_x and d_y for proposed method under $M_t \in \{9, 25, 64\}$ and classical method for high dynamic range, the ARMP 3D curves are plotted in Fig. 7. As anticipated, the symmetric ARMP curves arise due to the symmetry property of the LED array in both the x and y axes.

To show the impact of LED numbers, the ARMP versus M_t is depicted in Fig. 8 for some high dynamic ranges between elements in the array. As seen, although by increasing M_t, the LED array physical length is running larger, the optimized ARMP has incremental functionality with M_t. It has resulted that in large LED array panels, considering both M_t and dx jointly, M_t has a dominant impact on the ARMP of proposed method.

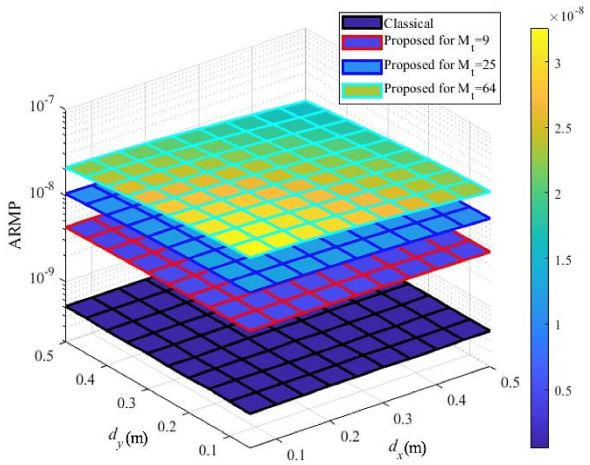

Fig. 7: The ARMP of proposed method under $M_t \in \{9, 25, 64\}$ and classical method versus high x and y axis dynamic range adjacent distances between LEDs in the array in.

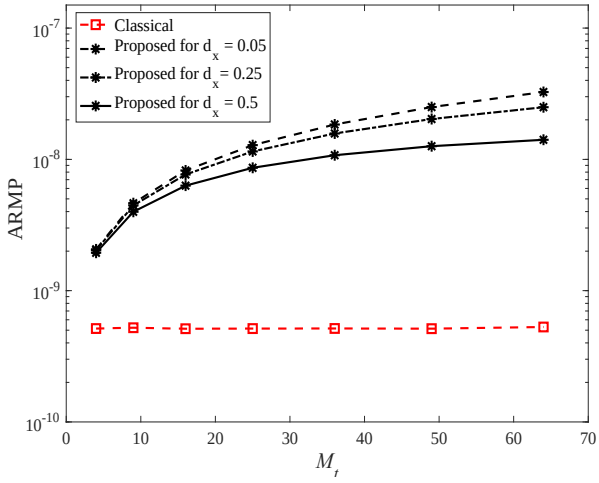

Fig. 8: The ARMP of classical and proposed algorithm versus number of LEDs in the array under some high dynamic range between elements in the array.

Finally, the performance of proposed and classical methods under different work plane heights is studied. To this end, we vary the work plane from the floor up to the height of 1m. We set d_x = 0.05m and $M_t \in \{9, 25, 64\}$ in our simulations. The result is shown in Fig. 9 in which the horizontal axis is the work plane height from the floor. As expected, by moving the work plane from the floor the ARMP for both proposed and classical methods increases. This is due to the fact that by increasing work plane height, the

distance between user locations and the LED array decreases which leads to a decrease in channel loss.

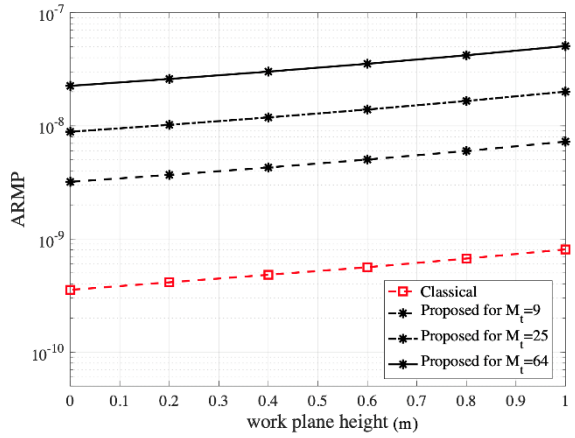

Fig. 9: The ARMP the ARMP of classical and proposed algorithm versus work plane height under different number of LEDs in the array.

D. Circular LED Array

This section aims to assess the performance of the proposed method in relation to various LED array configurations, specifically focusing on the ARMP of methods applied to circular arrays. To this end, the algorithm is tested for various values of radius $r \in \{0.5, 1, 1.5\}$. The results are depicted in Fig. 10 where plots the ARMP vs number of LEDs of the array. As seen, similar to rectangular array, the ARMP curves are rising by increase of M_t.

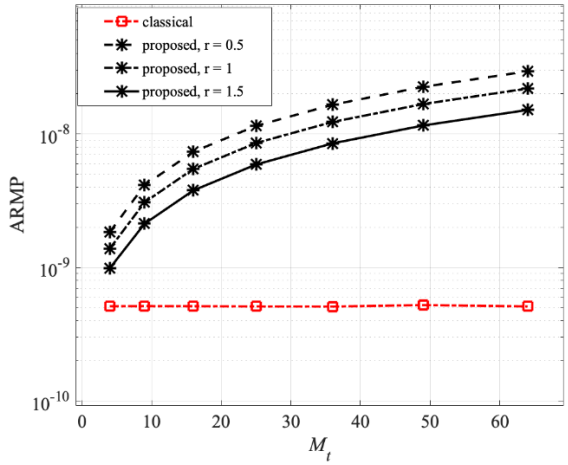

Fig. 10: The ARMP of classical and proposed algorithm versus number of LEDs in the array under some radiuses of the circle array.

E. Bit error rate analysis

For more investigation of the system performance, the bit error rate (BER) of the proposed method is compared with that of the classical method. Detection of public information at j-th user needs the value of the term $\boldsymbol{h}_j^T \boldsymbol{P}$ to be known. It is assumed that a pilot block of q symbols is broadcast at the first so the j-th user can estimate the relevant value of $\boldsymbol{h}_j^T \boldsymbol{P}$. Then, the main public information bits are modulated with usual on-off keying non-return to zero (NRZ) scheme then broadcast to all users. At the receiver side, each user detects the public information bits using the Maximum-Likelihood criterion based on the estimation of term $\boldsymbol{h}_j^T \boldsymbol{P}$ as

$$\hat{\boldsymbol{s}}_{\boldsymbol{ML}} = \underset{\boldsymbol{s}\epsilon\mathcal{S}}{\operatorname{argmin}} \left| r_j - \boldsymbol{h}_j^T \boldsymbol{P}\boldsymbol{s} \right|^2, \tag{14}$$

where $\mathcal{S}$ indicates the set of all possible values of vector $\boldsymbol{s}$. The mean BER of 15 users distributed uniformly in the work plane versus M_t with noise variance $\sigma^2 = 2 \times 10^{-7}$ is plotted in Fig. 11. As seen, the BER values of proposed method is fall with increase on M_t due to increase of ARMP in similar scenario.

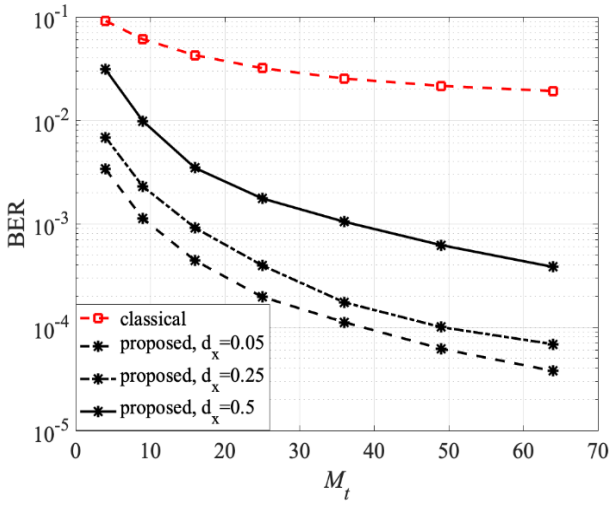

Fig. 11: The BER values versus M_t for classical and proposed method with different $d_x \in \{0.05, 0.25, 0.5\}$.

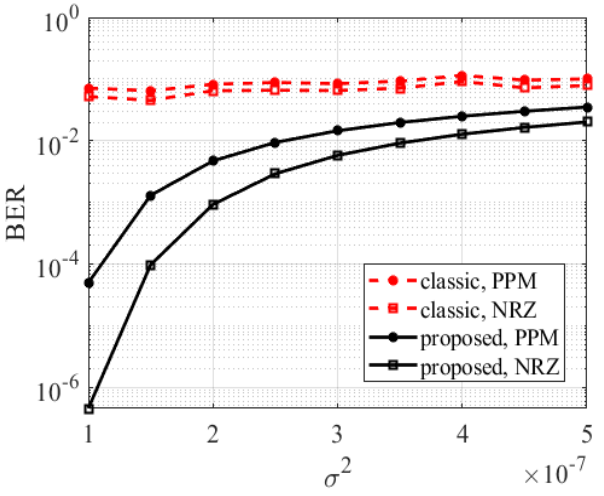

Fig. 12: The BER of proposed and classical methods versus noise variance under PPM and NRZ modulations.

Fig. 12 compares the performance of system under NRZ and pulse position modulation (PPM) versus noise variance for both proposed and classical methods under M_t = 9, d = 0.02 m. As seen, the BER values of the proposed methods encouragingly outperforms the classical method. Comparing the results, NRZ modulation outperforms than the PPM one.

Conclusion

In this research, we proposed an omnidirectional precoding for transmitting the public signals in MU-MIMO-VLC system. For this purpose, we proposed an optimization problem which maximizes the received mean power constrained with equal transmission mean power of LEDs in the array. In our formulation the constraint is in the form of manifold therefore a gradient method projected on the manifold is designed to solve the problem. We considered the ARMP parameter to investigate the performance of the system under varying some simulation parameters such as LED numbers in the array, distance between LEDs, and height of work plane from the floor. Simulation results has shown that the proposed omnidirectional precoding leads to higher ARMP values with respect to the classical method in all simulation scenarios.

Author Contributions

The present article is the outcome of a joint endeavor by H. Alizadeh and M. Atashbar. H. Alizadeh took the lead in drafting the manuscript, whereas M. Atashbar handled the execution of the simulations. Furthermore, both contributed to the analysis of the simulation outcomes.

Acknowledgment

The authors would like to thank the editor and anonymous reviewers.

Conflict of interest

The authors declare no potential conflict of interest regarding the publication of this work. In addition, the ethical issues including plagiarism, informed consent, misconduct, data fabrication and, or falsification, double publication and, or submission, and redundancy have been completely witnessed by the authors.

Abbreviations

VLC	Visible Light Communication
MU-MIMO	Multi-User Multiple-Input-Multiple-Output
CSI	Channel State Information
ARMP	Average of Received Mean Power
LoS	Line of Sight

References

[1] S. Aboagye, A. R. Ndjiongue, T. M. Ngatched, O. A. Dobre, H. V. Poor, "RIS-assisted visible light communication systems, A tutorial," IEEE Commun. Surv. Tutorials, 25(1): 251-288, 2022.

[2] W. Jiang, F. L. Luo, 6G Key Technologies: A Comprehensive Guide, John Wiley & Sons, 2023.

[3] H. S. R Hujijo, M. Ilyas, "Enhancing spectral efficiency with low complexity filtered-orthogonal frequency division multiplexing in visible light communication system," ETRI J., 46(6): 1007-1019, 2024.

[4] L. E. M. Matheus, A. B. Vieira, L. F. Vieira, M. A. Vieira, O. Gnawali, "Visible light communication: concepts, applications and challenges," IEEE Commun. Surv. Tutorials, 21(4): 3204-3237, 2019.

[5] E. G. Larsson, O. Edfors, F. Tufvesson, T. L. Marzetta, "Massive MIMO for next generation wireless systems," IEEE Commun. Mag., 52(2):186-195, 2014.

[6] E. Castaneda, A. Silva, A. Gameiro, M. Kountouris, "An overview on resource allocation techniques for multi-user MIMO systems," IEEE Commun. Surv. Tutorials, 19(1):239-284, 2016.

[7] J. Lian, M. Brandt-Pearce, "Multiuser visible light communication systems using OFDMA," J, Lightwave Technol., 38(21):6015-6023, 2020.

[8] C. Chen, W. D. Zhong, D. Wu, "On the coverage of multiple-input multiple-output visible light communications," J. Opt. Commun. Networking, 9(9): D31-D41, 2017.

[9] F. Xing, S. He, V. C. Leung, H. Yin, "Energy efficiency optimization for rate-splitting multiple access-based indoor visible light communication networks," IEEE J. Sel. Areas Commun., 40(5): 1706-1720, 2022.

[10] C. Wang, Y. Yang, Z. Yang, C. Feng, J. Cheng, C. Guo, "Joint SIC-based Precoding and Sub-connected architecture design for MIMO VLC systems," IEEE Trans. Commun., 71(2): 1044-1058, 2023.

[11] F. R Castillo-Soria, C Gutierrez, F. M Maciel-Barboza, V. I Rodriguez Abdala, J Datta, "Relay-assisted multiuser MIMO-DQSM system for correlated fading channels," ETRI J., 46(2): 184-193, 2024.

[12] F. Yang, Y. Dong, "Joint probabilistic shaping and beamforming scheme for MISO VLC systems," IEEE Wireless Commun. Lett., 11(3): 508-512, 2021.

[13] Y. Hong, J. Chen, Z. Wang, C. Yu, "Performance of a precoding MIMO system for decentralized multiuser indoor visible light communications," IEEE Photonics J., 5(4): 7800211-7800211, 2013.

[14] S. T. Duong, T. V. Pham, C. T. Nguyen, A. T. Pham, "Energy-efficient precoding designs for multi-user visible light communication systems with confidential messages," IEEE Trans. Green Commun. Networking, 5(4): 1974-1987, 2021.

[15] Q. Zhao, Y. Fan, B. Kang, "A joint precoding scheme for indoor downlink multi-user MIMO VLC systems," Opt. Commun., 403: 341-346, 2017.

[16] H. Marshoud, P. C. Sofotasios, S. Muhaidat, B. S. Sharif, G. K. Karagiannidis, "Optical adaptive precoding for visible light communications," IEEE Access, 6: 22121-22130, 2018.

[17] H. Ma, L. Lampe, S. Hranilovic, "Robust MMSE linear precoding for visible light communication broadcasting systems," in Proc. 2013 IEEE Globecom Workshops (GC Wkshps), 2013.

[18] T. V. Pham, H. Le-Minh, A. T. Pham, "Multi-user visible light communication broadcast channels with zero-forcing precoding," IEEE Trans. Commun., 65(6): 2509-2521, 2017.

[19] N. T. Le, Y.M. Jang, "Broadcasting MAC protocol for IEEE 802.15. 7 visible light communication," in Proc. 2013 Fifth International Conference on Ubiquitous and Future Networks (ICUFN), 2013.

[20] Y. Mao, O. Dizdar, B. Clerckx, R. Schober, P. Popovski, H. V. Poor, "Rate-splitting multiple access: Fundamentals, survey, and future research trends," IEEE Commun. Surv. Tutorials, 24(4): 2073-2126, 2022.

[21] S. A. Naser, P. C. Sofotasios, S. Muhaidat, M. Al-Qutayri, "Rate-splitting multiple access for indoor visible light communication networks," in Proc. 2021 IEEE Wireless Communications and Networking Conference Workshops (WCNCW), 2021.

[22] M. Dai, B. Clerckx, D. Gesbert, G. Caire, "A rate splitting strategy for massive MIMO with imperfect CSIT," IEEE Trans. Wireless Commun., 15(7): 4611-4624, 2016.

[23] L. Mavarayi, M. Atashbar, "Omnidirectional precoding for massive MIMO with uniform rectangular array in presence of mutual coupling," Digital Signal Process., 130: 103717, 2022.

[24] X. Men, T. Liu, Y. Li, M. Liu, "Constructions of 2-D golay complementary array sets with flexible array sizes for omnidirectional precoding in massive MIMO," IEEE Commun. Lett., 27(5): 1302-1306, 2023.

[25] S. Yahia, Y. Meraihi, A. Ramdane-Cherif, A. B. Gabis, D. Acheli, H. Guan, "A survey of channel modeling techniques for visible light communications," J. Network Comput. Appl., 194: 103206, 2021.

[26] Z. Ghassemlooy, W. Popoola, S. Rajbhandari, Optical wireless communications: system and channel modelling with Matlab®, CRC press, 2019.

[27] Z. Wang, Q. Wang, W. Huang, Z. Xu, Visible light communications: modulation and signal processing, John Wiley & Sons, 2017.

[28] E. Telatar, "Capacity of multi-antenna Gaussian channels," Eur. Trans. Telecommun., 10(6): 585-595, 1999.

[29] X. Meng, X. Gao, X. G. Xia, "Omnidirectional precoding based transmission in massive MIMO systems," IEEE Trans. Commun., 64(1): 174-186, 2015.

[30] P. A. Absil, R. Mahony, R. Sepulchre, Optimization algorithms on matrix manifolds, Princeton University Press, 2008.

[31] J. H. Manton, "Geometry, manifolds, and nonconvex optimization: How geometry can help optimization," IEEE Signal Process. Mag., 37(5): 109-119, 2020.

[32] G. A. Seber, A matrix handbook for statisticians, John Wiley & Sons, 2008.

Biographies

Hamed Alizadeh Ghazijahani was born in Ghazijahan, Iran in 1988. He completed his B.Sc., M.Sc., and Ph.D. degrees in electrical engineering, with a focus on telecommunications, at the University of Tabriz, Iran, in the years 2010, 2013, and 2019, respectively. In 2020, he took on the role of assistant professor at Azarbaijan Shahid Madani University. His research primarily explores optical and wireless communication systems and networks.

- E-mail: hag@azaruniv.ac.ir
- ORCID: 0000-0002-2438-7700
- Web of Science Researcher ID: AGS-4002-2022
- Scopus Author ID: 36863455200
- Homepage: http://pajouhesh.azaruniv.ac.ir/_Pages/ResearcherEn.aspx?ID=9914

Mahmoud Atashbar was born in Marand, in the East Azarbijan province of Iran in 1979. He received his BS degree in electrical engineering from the School of Electrical Engineering, Sahand University of Technology, Tabriz, Iran, in 2003, and his MS and Ph.D. degree in telecommunication engineering from the school of electrical engineering, Iran University of Science and Technology, Tehran, Iran, in 2006 and 2013, respectively. Since 2013, he has been with the Department of Electrical Engineering, Azarbaijan Shahid Madani University, Tabriz, Iran, where he is now an assistant professor. His research interests include wireless communication and communication systems.

- Email: atashbar@azaruniv.ac.ir
- ORCID: 0000-0003-3721-4128
- Web of Science Researcher ID: GRE-9721-2022
- Scopus Author ID: 56035037500
- Homepage: http://pajouhesh.azaruniv.ac.ir/_Pages/Researcher.aspx?ID=1040

How to cite this paper:
H. Alizadeh Ghazijahani, M. Atashbar, "A public information precoding for MIMO visible light communication system based on manifold optimization," J. Electr. Comput. Eng. Innovations, 13(2): 307-316, 2025.

DOI: 10.22061/jecei.2024.11251.782

URL: https://jecei.sru.ac.ir/article_2240.html